ADVANCED MATERIALS

Supporting Information

for *Adv. Mater.,* DOI: 10.1002/adma.202104863

Electrically Tunable and Dramatically Enhanced Valley-Polarized Emission of Monolayer WS_2 at Room Temperature with Plasmonic Archimedes Spiral Nanostructures

Wei-Hsiang Lin, Pin Chieh Wu, Hamidreza Akbari, George R. Rossman, Nai-Chang Yeh,* and Harry A. Atwater**

WILEY-VCH

Supporting Information

Electrically Tunable and Dramatically Enhanced Valley-Polarized Emission of Monolayer WS_2 at Room Temperature with Plasmonic Archimedes Spiral Nanostructures

Wei-Hsiang Lin, Pin Chieh Wu, Hamidreza Akbari, George. R. Rossman, Nai-Chang Yeh* and Harry A. Atwater**

Wei-Hsiang Lin, Hamidreza Akbari, Prof. Harry A. Atwater
Department of Applied Physics, California Institute of Technology, Pasadena, CA 91125, USA
E-mail: haa@caltech.edu and whlin@alumni.caltech.edu

Prof. Pin Chieh Wu
Department of Photonics, National Cheng Kung University, Tainan 70101, Taiwan

Prof. George. R. Rossman
Department of Geological and Planetary Sciences, California Institute of Technology, Pasadena, CA 91125, USA

Prof. Nai-Chang Yeh
Department of Physics, California Institute of Technology, Pasadena, CA 91125, USA
E-mail: ncyeh@caltech.edu

Supporting Information 1.

We have characterized our single crystalline WS_2 samples using Raman spectroscopy and X-ray photoelectron spectroscopy (XPS), and the representative data are summarized below.

To demonstrate the crystallinity of single crystalline WS_2, we performed Raman spectroscopic studies of the A_{1g} and E^1_{2g} modes using a 514.3 nm laser (2.41 eV) as the excitation source, and a representative spectrum is shown in Figure S1.

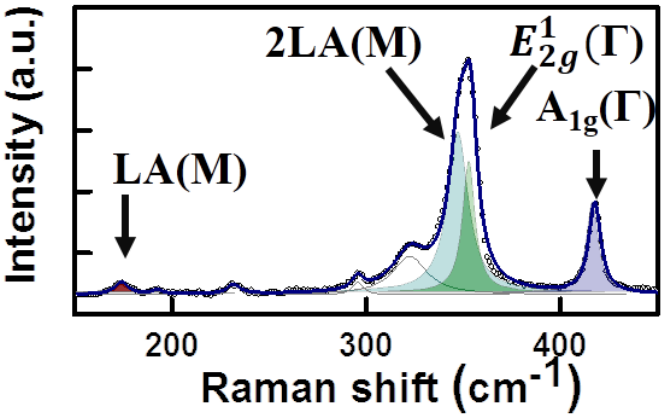

Figure S1. Raman spectrum of a monolayer WS_2, showing the A_{1g} and E^1_{2g} optical phonon modes, and the LA (M) mode associated with the longitudinal acoustic phonon at the M point of the Brillouin zone, which may be considered as an indicator of the sample quality.

X-ray photoelectron spectroscopy (XPS) was also conducted to examine the chemical composition and valence states of monolayer WS_2 transferred to Au (111) / mica substrates. The core level spectra were calibrated via fitting adventitious carbon at 284.8 eV. The high-resolution spectra of W 4f and S 2p peaks are shown in Figure S2. For 2H-phase WS_2, the corresponding binding energies of the W $4f_{7/2}$ and W $4f_{5/2}$ peaks were found to locate at 32.15

and 34.31 eV, respectively, and the binding energies for the S $2p_{3/2}$ and S $2p_{1/2}$ peaks were located at 162.87 and 163.07 eV, respectively. These values are all consistent with those reported previously in literature.

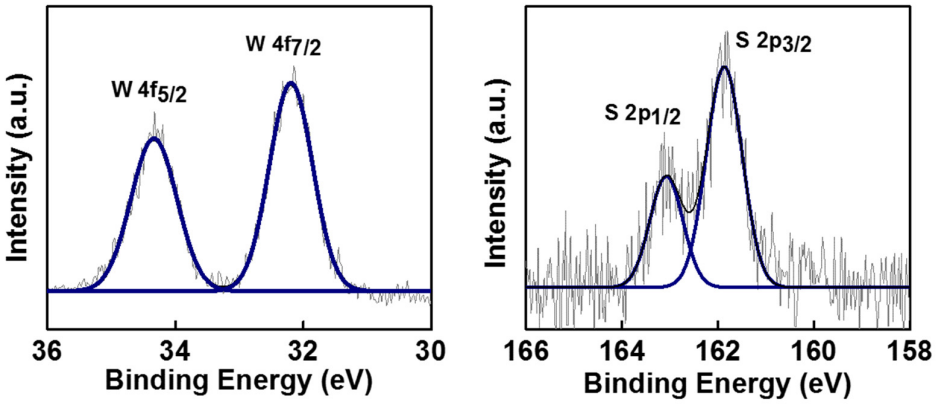

Figure S2. XPS of a monolayer WS_2, showing the W $4f_{7/2}$ and W $4f_{5/2}$ peaks in the left spectrum and the S $2p_{3/2}$ and S $2p_{1/2}$ peaks in the right spectrum.

Supporting Information 2.

The total decay rate of the as-grown monolayer WS_2 without coupling to the plasmonic nanostructures is:

$$\gamma_{off} = \gamma_R + \gamma_{NR}, \tag{1}$$

where γ_R and γ_{NR} are the radiative and nonradiative decay rates, respectively. The coupling to plasmonic nano-cavities enhances the radiative rate by the Purcell effect and induces a new decay channel through metallic losses with a rate γ_M. Therefore, the total decay rate of the coupled monolayer WS_2 can be expressed as:

$$\gamma_{on} = (F_p + 1)\gamma_R + \gamma_{NR} + \gamma_M \ , \tag{2}$$

where F_p is the Purcell factor that enhances the radiative decay rate. Therefore,

$$\frac{\gamma_{on}}{\gamma_{off}} = \frac{(F_p + 1)\gamma_R + \gamma_{NR} + \gamma_M}{\gamma_R + \gamma_{NR}} . \tag{3}$$

In order to determine the underlying Purcell factor from the measured rates, we note that the quantum yield η is defined as the ratio of the number of photons emitted to the number of photons absorbed:

$$\eta_{off} = \frac{\gamma_R}{\gamma_R + \gamma_{NR}} \ , \tag{4}$$

$$\eta_{on} = \frac{(F_p + 1)\gamma_R}{\gamma_R + \gamma_{NR}} \ , \tag{5}$$

$$\gamma_{on} - \gamma_{off} = F_p \gamma_R + \gamma_M \ . \tag{6}$$

Therefore, the metallic-loss corrected Purcell factor F_p is given by:

$$F_p = \left(\frac{F_p \gamma_R}{F_p \gamma_R + \gamma_M} \right) \left(\frac{\gamma_{on}}{\gamma_{off}} - 1 \right) \eta_{off}^{-1} . \tag{7}$$

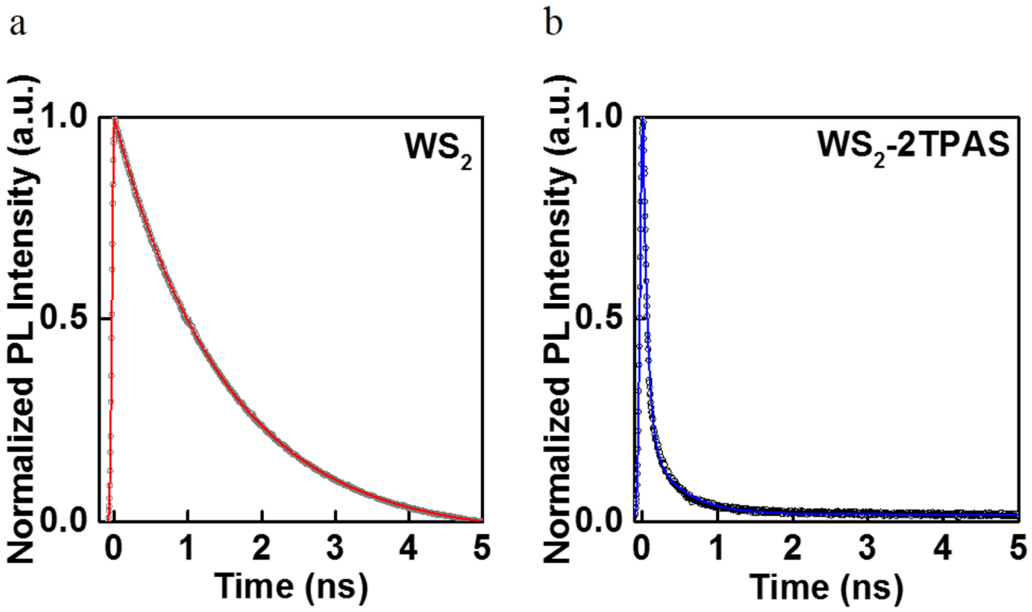

Figure S3. Time-resolved PL decay profile of a) WS_2 and b) WS_2-2TRHPAS.

Supporting Information 3.

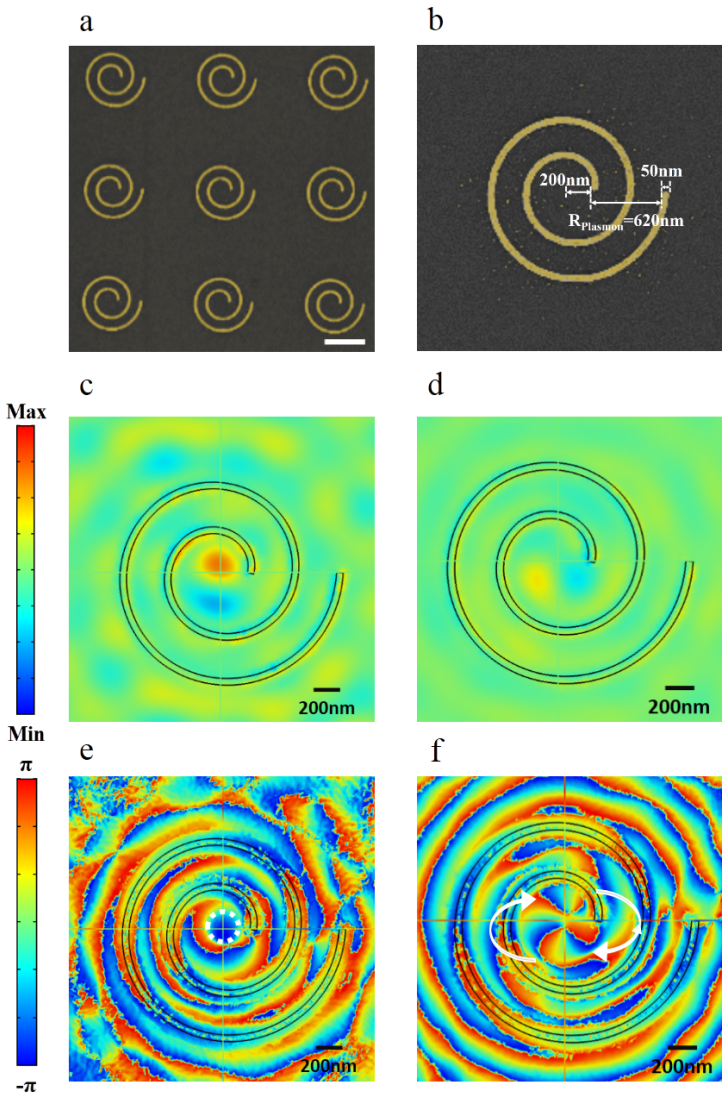

Figure S4. Geometric structure and E-field distribution of WS_2-2TRHPAS heterostructure. a) SEM image of 2TRHPAS. (Scale bar: 1.25μm). b) The spiral width, inner radius and pitch are 50 nm, 200 nm, and 310 nm, respectively. c) Near-field of E_z in the x-y plane with a focusing spot under the RCP excitation. d) Near-field of E_z in the x-y plane with focusing spot under LCP excitation. e) Phase map of E_z in the x-y plane for RCP excitation. f) Phase map of E_z in the x-y plane for LCP excitation.

Supporting Information 4.

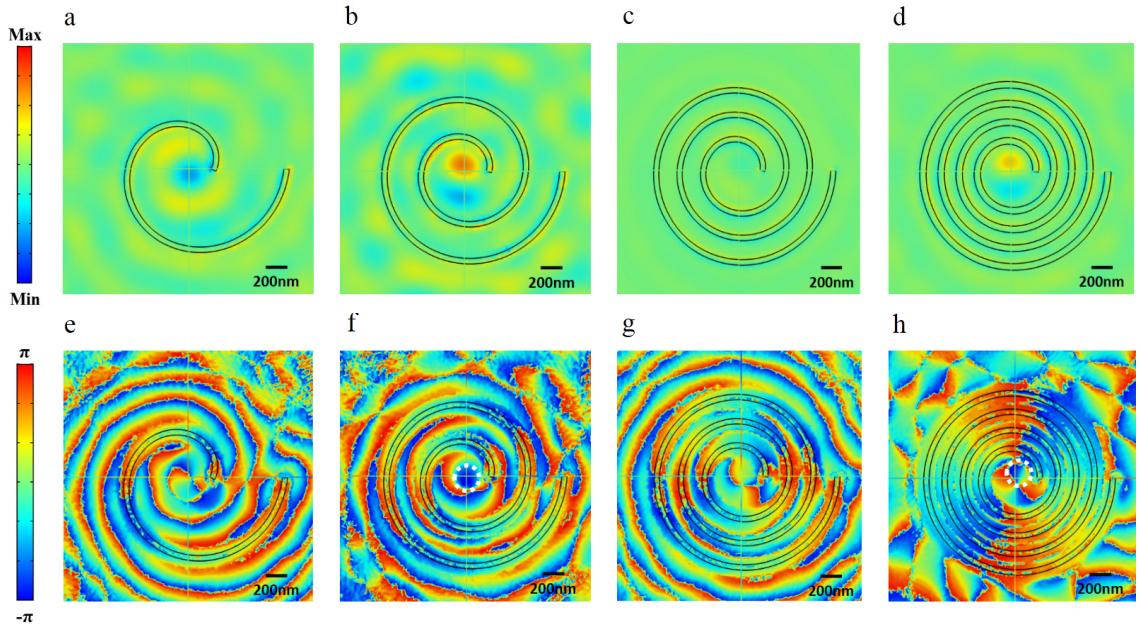

Figure S5. Electric field (images) of WS_2 with a) 1-turn, b) 2-turn, c) 3-turn, and d) 4-turn RHPAS under RCP excitation. Focusing point at the center of the RHPAS structure can be obtained from 2- and 4-turn spirals. Corresponding phase distribution of WS_2 with e) 1-turn, f) 2-turn, g) 3-turn, and h) 4-turn RHPAS under RCP excitation.

Supporting Information 5.

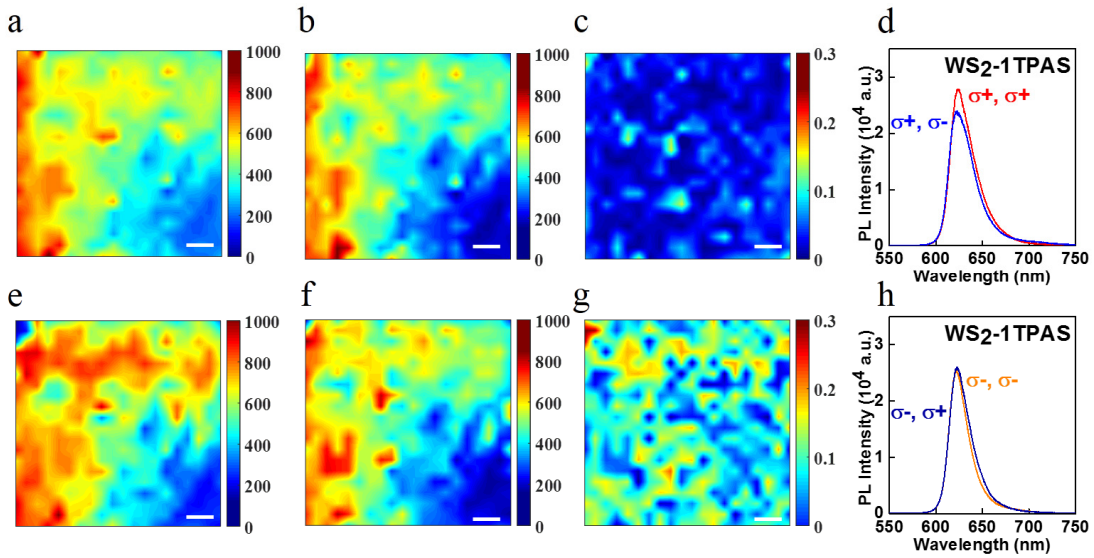

Figure S6. a) – d) Circularly polarized emission from as-grown monolayer WS_2 with 1-turn PAS array under 514nm σ+ excitation: a) σ+ polarized emission and b) σ- polarized emission intensity mapping. c) A spatial map for the degree of valley polarization (DVP) in a WS_2 with 1-turn PAS array. d) Representative σ+ (red) and σ- (blue) PL intensity spectra taken at room temperature on the WS_2 with 1-turn PAS array. e) – h) Monolayer WS_2 with 1-turn PAS array under 514nm σ- excitation: e) σ+ polarized emission and f) σ- polarized emission intensity mapping. g) A spatial map for the degree of valley polarization (DVP) in a WS_2 with 1-turn PAS array. h) Representative σ+ (navy) and σ- (orange) PL intensity spectra taken at room temperature on the WS_2 with 1-turn PAS array.

Supporting Information 6.

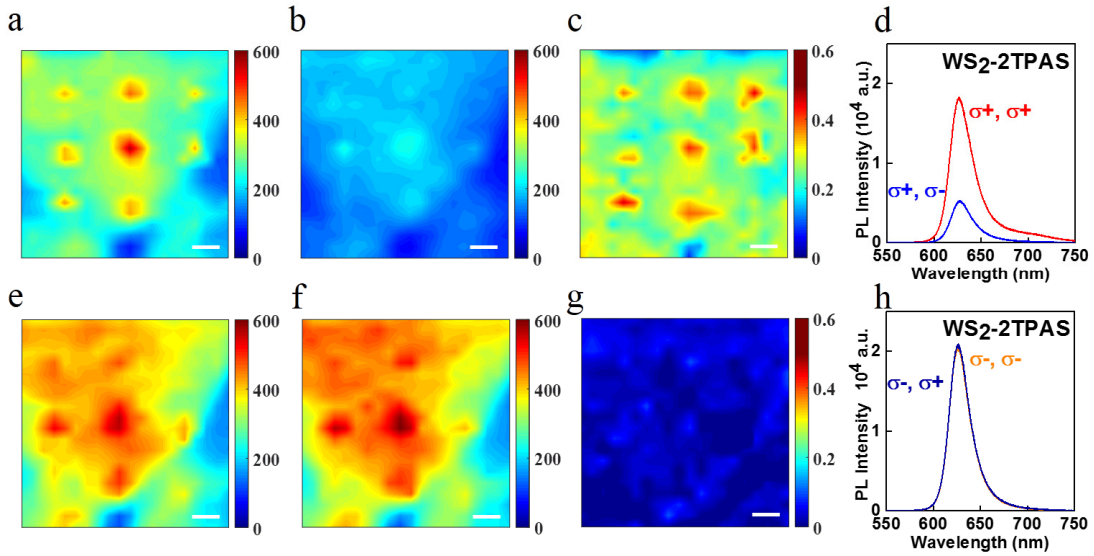

Figure S7. a) – d) Circularly polarized emission from as-grown monolayer WS_2 with 2-turn PAS array under 514nm σ+ excitation: a) σ+ polarized emission and b) σ– polarized emission intensity mapping. c) A spatial map for the degree of valley polarization (DVP) in a WS_2 with 2-turn PAS array. d) Representative σ+ (red) and σ- (blue) PL intensity spectra taken at room temperature on the WS_2 with 2-turn PAS array. e) – h) Monolayer WS_2 with 2-turn PAS array under 514nm σ– excitation: e) σ+ polarized emission and f) σ– polarized emission intensity mapping. g) A spatial map for the degree of valley polarization (DVP) in a WS_2 with 2-turn PAS array. h) Representative σ+ (navy) and σ– (orange) PL intensity spectra taken at room temperature on the WS_2 with 2-turn PAS array.

Supporting Information 7.

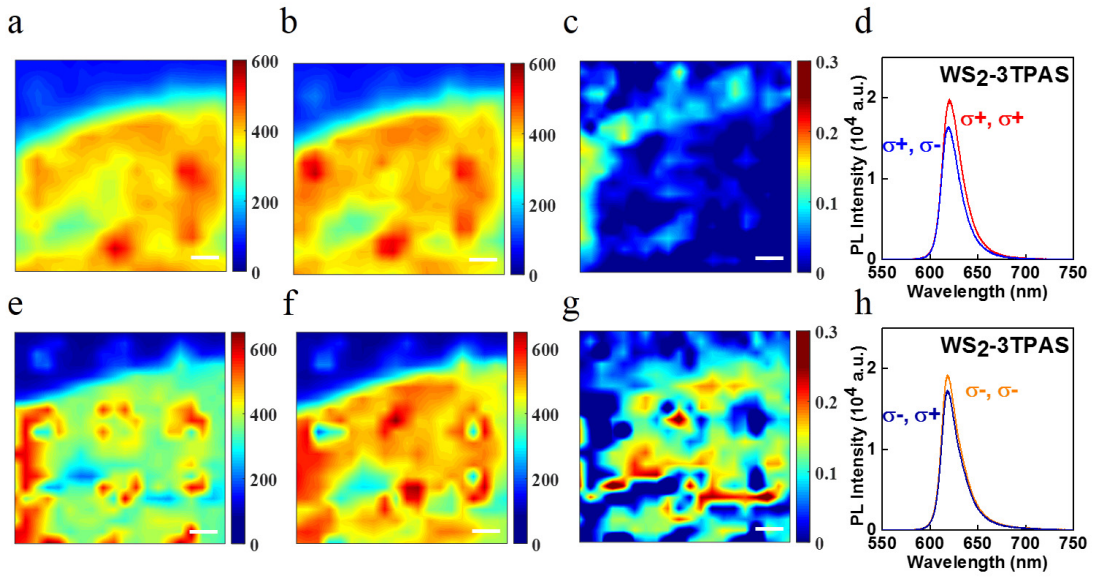

Figure S8. a) – d) Circularly polarized emission from as-grown monolayer WS_2 with 3-turn PAS array under 514nm σ+ excitation: a) σ+ polarized emission and b) σ– polarized emission intensity mapping. c) A spatial map for the degree of valley polarization (DVP) in a WS_2 with 3-turn PAS array. d) Representative σ+ (red) and σ– (blue) PL intensity spectra taken at room temperature on the WS_2 with 3-turn PAS array. e) – h) Monolayer WS_2 with 3-turn PAS array under 514nm σ– excitation: e) σ+ polarized emission and f) σ– polarized emission intensity mapping. g) A spatial map for the degree of valley polarization (DVP) in a WS_2 with 3-turn PAS array. h) Representative σ+ (navy) and σ– (orange) PL intensity spectra taken at room temperature on the WS_2 with 3-turn PAS array.

Supporting Information 8.

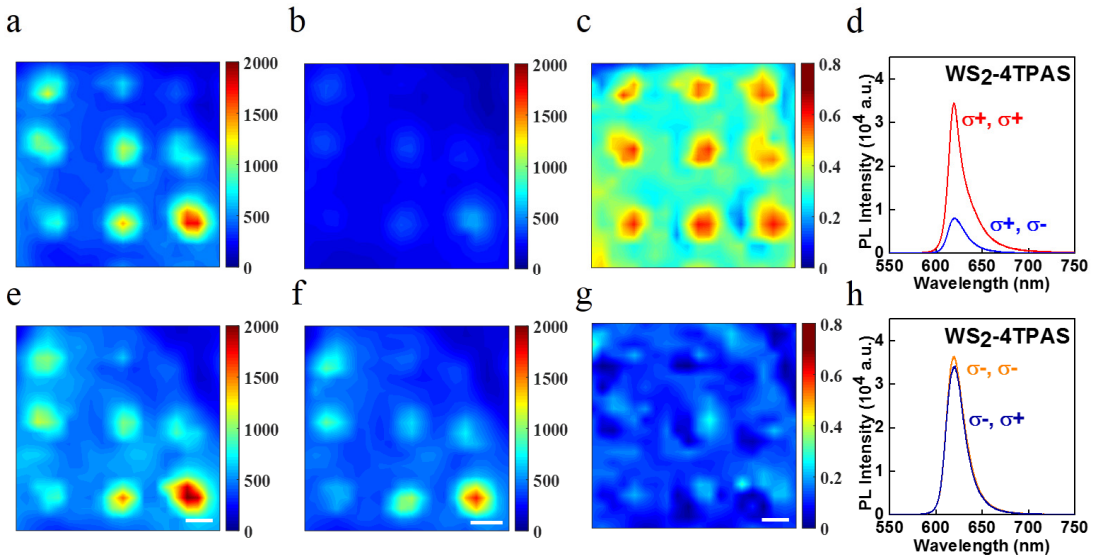

Figure S9. a) – d) Circularly polarized emission from as-grown monolayer WS_2 with 4-turn PAS array under 514nm σ+ excitation: a) σ+ polarized emission and b) σ– polarized emission intensity mapping. c) A spatial map for the degree of valley polarization (DVP) in a WS_2 with 4-turn PAS array. d) Representative σ+ (red) and σ– (blue) PL intensity spectra taken at room temperature on the WS_2 with 4-turn PAS array. e) – h) Monolayer WS_2 with 4-turn PAS array under 514nm σ- excitation: e) σ+ polarized emission and f) σ– polarized emission intensity mapping. g) A spatial map for the degree of valley polarization (DVP) in a WS_2 with 4-turn PAS array. h) Representative σ+ (navy) and σ– (orange) PL intensity spectra taken at room temperature on the WS_2 with 4-turn PAS array.

Supporting Information 9.

To investigate the effect of the plasmonic Archimedes spiral (PAS) resonance wavelength ($R_{Plasmon}$) on the enhancement of the DVP, we performed measurements of three different resonance wavelengths. The resonance wavelengths of the PAS nanostructures are $R_{Plasmon}$ = 310 nm (2.42×10^{14} Hz), 620 nm (4.84×10^{14} Hz) and 930 nm (7.26×10^{14} Hz), respectively, and the corresponding photoluminescence (PL) spectra and the DVP values are shown in Figure S10 below. These studies suggest that the best room temperature DVP enhancement occurred when the resonance wavelength $R_{Plasmon}$ of the PAS nanostructures is 620 nm, which coincided with the neutral A-exciton emission wavelength.

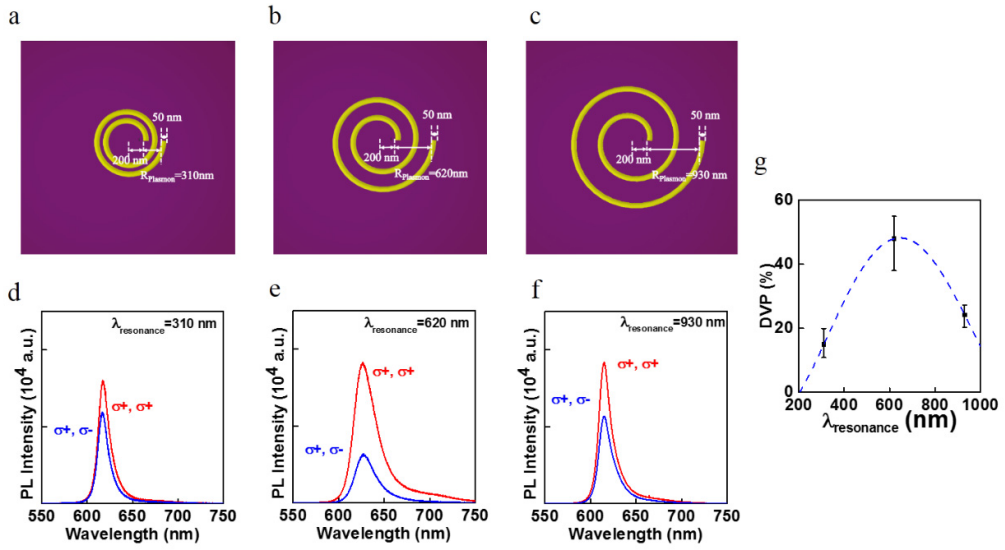

Figure S10. Schematics of the PAS nanostructures and the corresponding DVP. The spiral width and inner radius are 50 nm and 200 nm, respectively. The resonance wavelengths are a) 310 nm, b) 620 nm, and c) 930 nm, respectively. The corresponding σ+ (red) and σ- (blue) PL intensity spectra were shown in d-f). g) Summary of the three different resonance wavelengths corresponding to the DVP, showing the best DVP for the resonance wavelength 620 nm that coincides with the A-exciton emission wavelength.

Supporting Information 10.

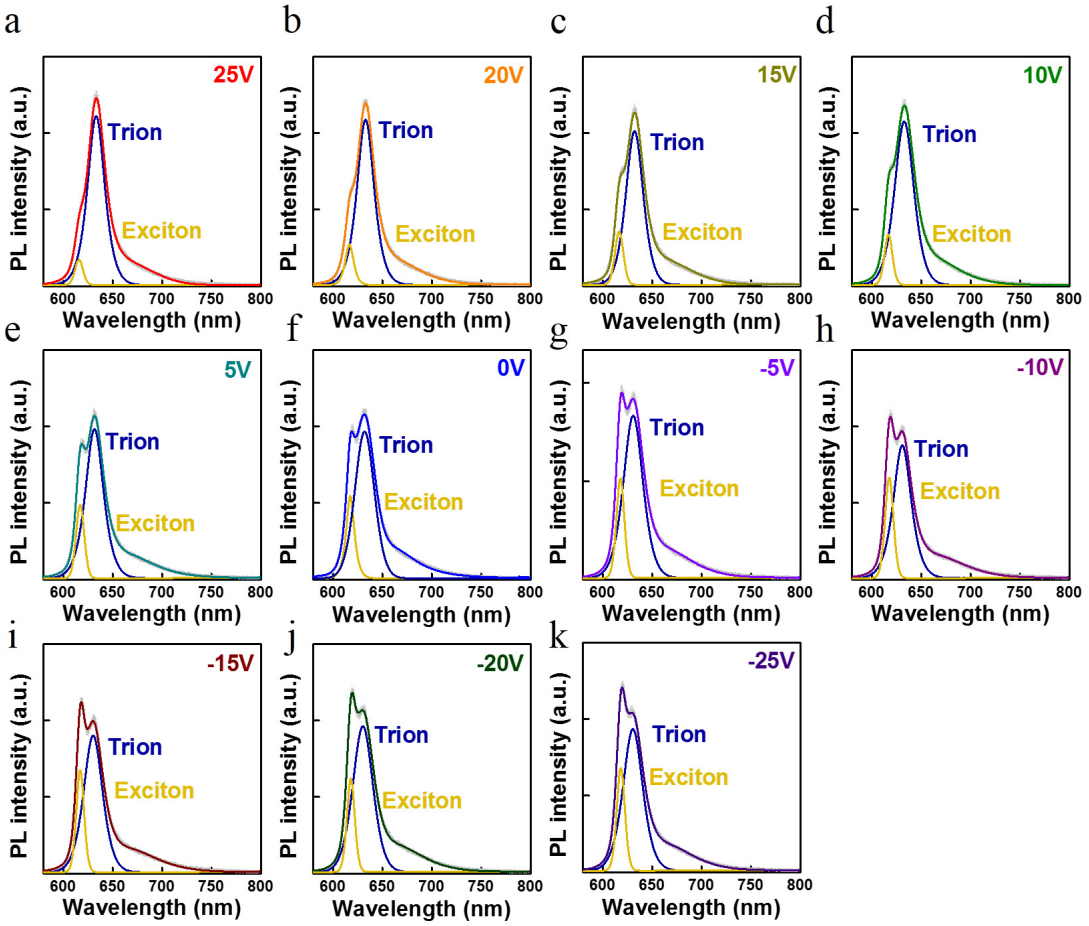

Figure S11. Gaussian−Lorentzian fitting of the electric tunning PL spectra of pure monolayer WS_2 under V_{Gate} = a) 25 V, b) 20 V, c) 15 V, d) 10 V, e) 5 V, f) 0, g) −5 V, h) −10 V, i) −15 V, j) −20 V, and k) −25 V. Two spectral components, the A-exciton (yellow line), and trion (navy line), were obtained by the Gaussian−Lorentzian fitting.

Supporting Information 11.

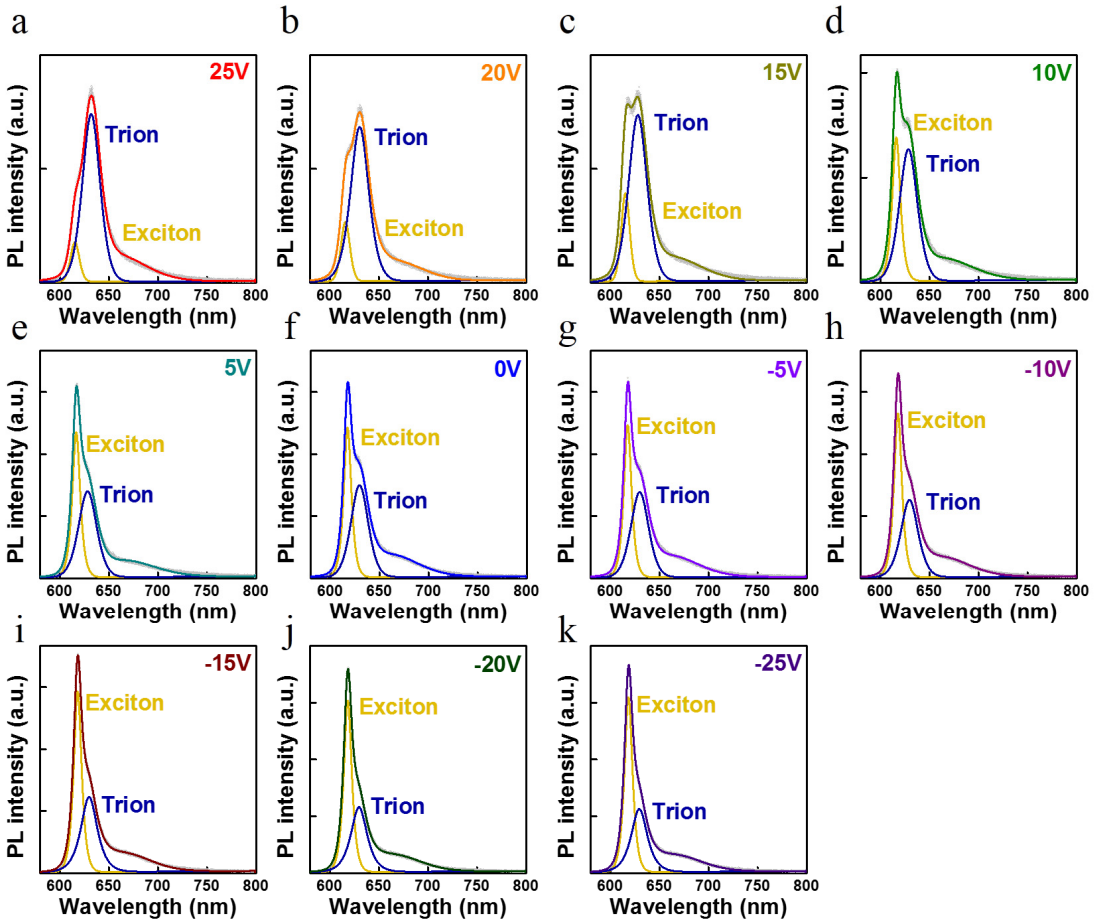

Figure S12. Gaussian−Lorentzian Fitting of the electric tunning PL spectra of WS_2-2TRHPAS under V_G = a) 25 V, b) 20 V, c) 15 V, d) 10 V, e) 5 V, f) 0, g) –5 V, h) –10 V, i) –15 V, j) –20 V, and k) –25 V. Two spectral components associated with the A-exciton (yellow line) and trion (navy line) were obtained by the Gaussian−Lorentzian fitting.

Supporting Information 12.

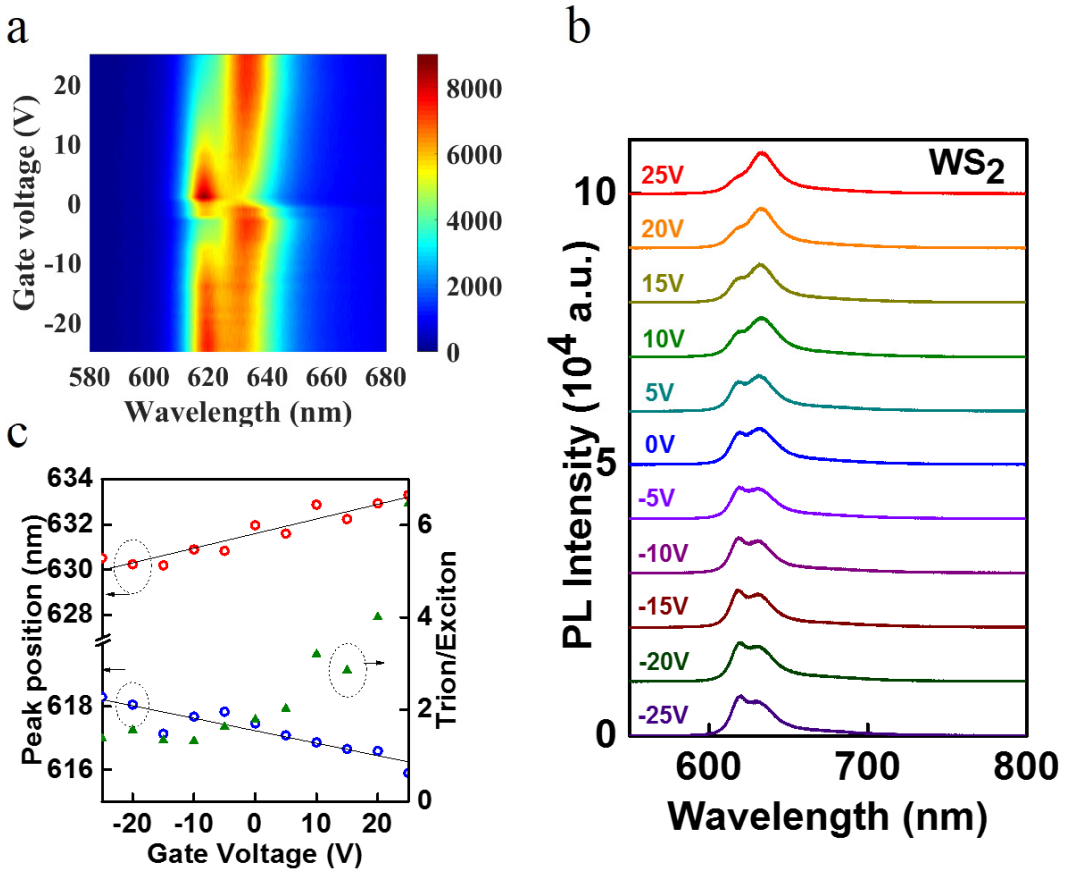

Figure S13. a) Contour plot of the PL spectra of 1L-WS_2 as a function of applied gate voltage (V_{Gate}) at RT. b) PL spectra at RT for V_{Gate} from –25 V to 25 V, with an increment of 5 V. c) Gate voltage dependence of the PL peak position of neutral exciton (blue) and trion (red) under V_{Gate} from –25 V to 25 V, together with the intensity ratio of trions and excitons (green) as a function of V_{Gate} from –25 V to 25 V.

Supporting Information 13.

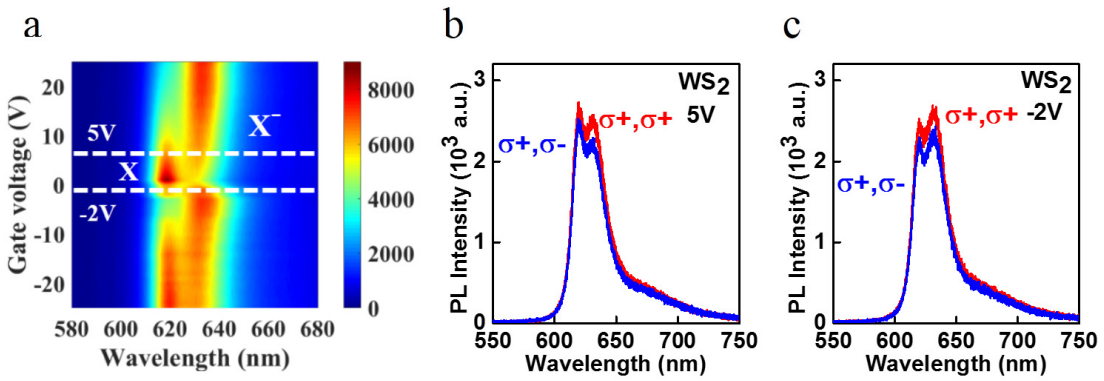

Figure S14. a) Contour plot of the PL spectra of 1L-WS_2 as a function of applied gate voltage (V_{Gate}) at RT. Polarization-resolved PL spectra under σ^+ (RCP) excitations for b) V_{Gate} = 5 V and c) V_{Gate} = -2 V.

Supporting Information 14.

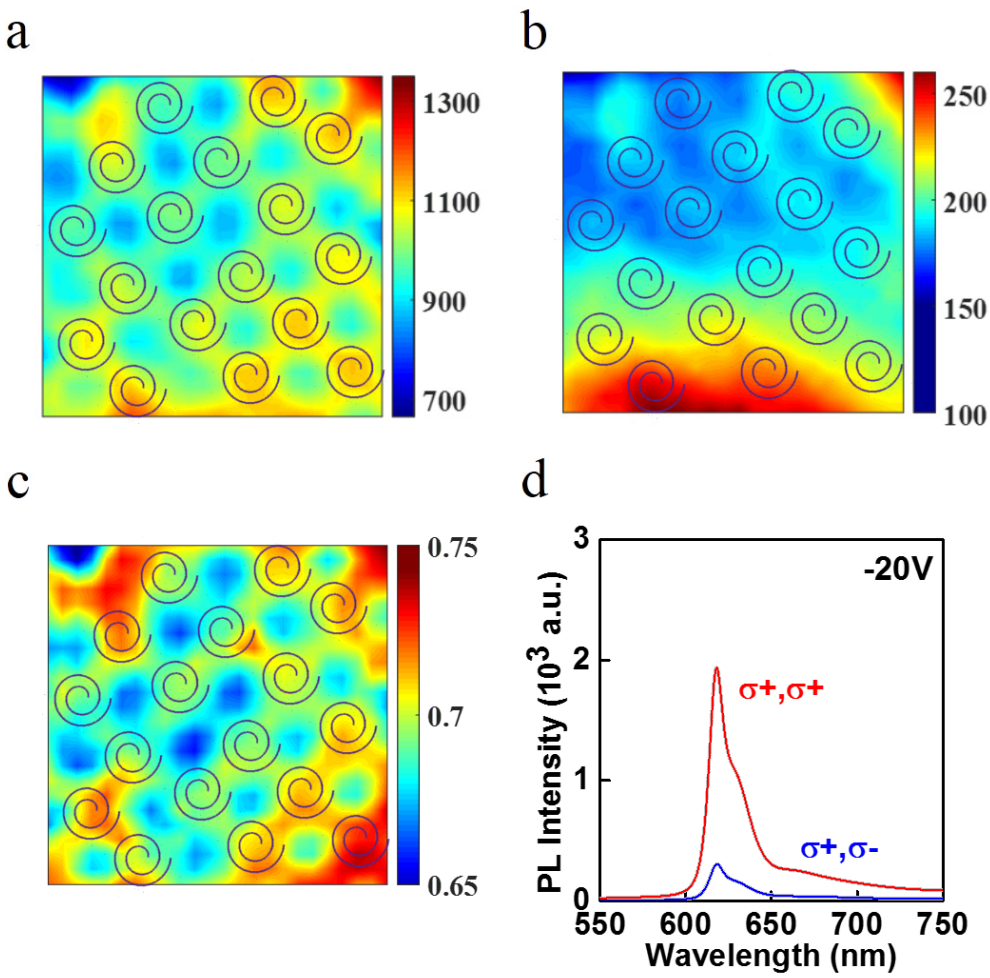

Figure S15. Electric tuning of circularly polarized emission from monolayer (1L) WS_2 with 2-turn right-handed (RH) PAS array under 514 nm σ+ excitation. a) σ+ polarized emission and b) σ– polarized emission intensity mapping under $V_{Gate} = -20$ V. c) A spatial map for the degree of valley polarization (DVP) in a 1L-WS_2 with 2TRHPAS array under $V_{Gate} = -20$ V. d) Representative σ+ (red) and σ- (blue) PL intensity spectra under $V_{Gate} = -20$ V taken at room temperature on the 1L-WS_2 with 2TRHPAS array.

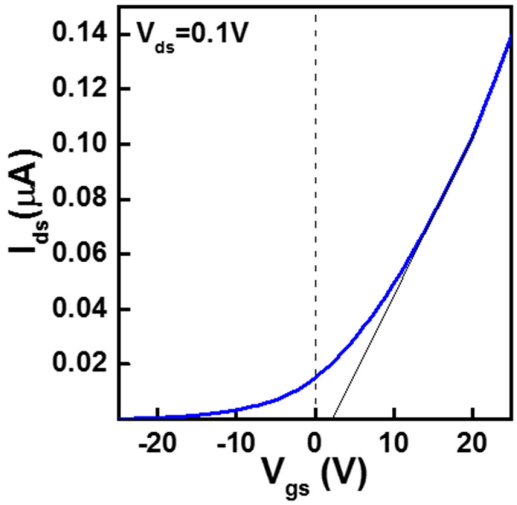

Figure S16. Transfer characteristic curve (I_{ds}-V_{gs}) of a WS_2-2TRHPAS heterostructure FET measured at a source-drain voltage V_{ds} = 0.1 V.